J. Fluid Mech. (1997), *vol.* 331, *pp.* 59–80

Regimes of coalescence and separation in droplet collision

By J. QIAN AND C. K. LAW

Department of Mechanical and Aerospace Engineering, Princeton University, Princeton, NJ 08544, USA

(Received 12 June 1995 and in revised form 26 April 1996)

An experimental investigation of the binary droplet collision dynamics was conducted, with emphasis on the transition between different collision outcomes. A series of time-resolved photographic images which map all the collision regimes in terms of the collision Weber number and the impact parameter were used to identify the controlling factors for different outcomes. The effects of liquid and gas properties were studied by conducting experiments with both water and hydrocarbon droplets in environments of different gases (air, nitrogen, helium and ethylene) and pressures, the latter ranging from 0.6 to 12 atm. It is shown that, by varying the density of the gas through its pressure and molecular weight, water and hydrocarbon droplets both exhibit five distinct regimes of collision outcomes, namely (I) coalescence after minor deformation, (II) bouncing, (III) coalescence after substantial deformation, (IV) coalescence followed by separation for near head-on collisions, and (V) coalescence followed by separation for off-centre collisions. The present result therefore extends and unifies previous experimental observations, obtained at one atmosphere air, that regimes II and III do not exist for water droplets. Furthermore, it was found that coalescence of the hydrocarbon droplets is promoted in the presence of gaseous hydrocarbons in the environment, suggesting that coalescence is facilitated when the environment contains vapour of the liquid mass. Collision at high-impact inertia was also studied, and the mechanisms for separation after coalescence are discussed based on time-resolved collision images. A coalescence/separation criterion defining the transition between regimes III and IV for the head-on collisions was derived and found to agree well with the experimental data.

1. Introduction

The phenomena of binary droplet collision are of interest to the studies of raindrop formation, nuclear fusion, and various spraying processes, especially those occurring in volume-limited internal combustion engines (Faeth 1977; O'Rourke & Bracco 1980). In particular, because of the dense nature of the droplet concentration immediately downstream of the fuel injector, droplet collision is expected to be a frequent event and can significantly modify the subsequent spray development and combustion characteristics.

Earlier studies on droplet collision (e.g. Adam & Linblad 1968; Park 1970; Brazier-Smith, Jennings & Latham 1972; Ashgriz & Poo 1990) have employed water droplets colliding in one atmosphere air because of the predominant interest in meteorological applications. Figure 1 schematically shows the various regimes for the collision outcome of water droplets in atmospheric air, where the Weber number We and impact parameter B are respectively defined, for identical droplets, as $2R\rho U^2/\sigma$ and $\chi/(2R)$,

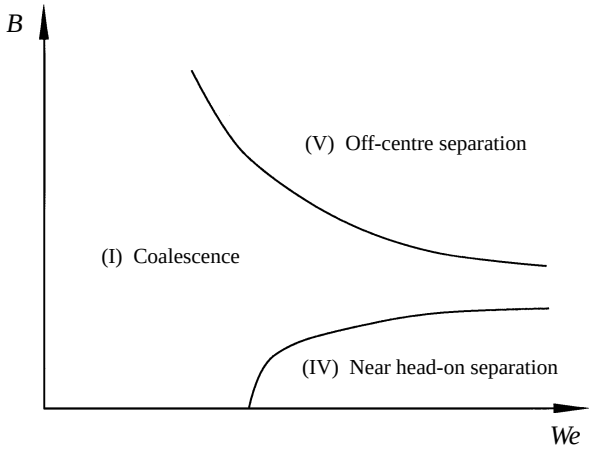

FIGURE 1. Schematic of various collision regimes of water droplets in 1 atm. air.

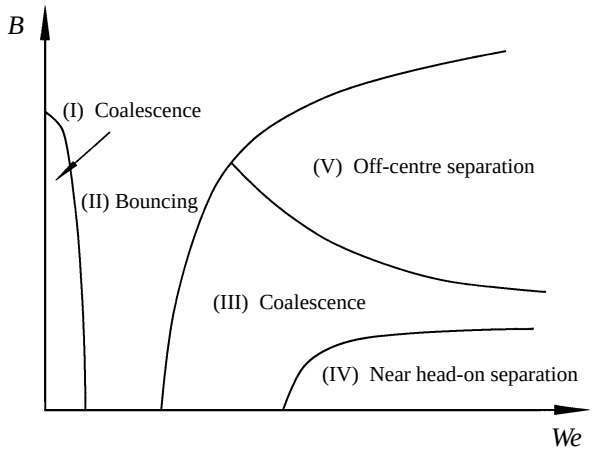

FIGURE 2. Schematic of various collision regimes of hydrocarbon droplets in 1 atm. air.

with R being the droplet radius, U the relative velocity, χ the projection of the separation distance between the droplet centres in the direction normal to that of U, and ρ and σ the density and surface tension of the liquid, respectively. Thus $B = 0$ and 1, respectively, designate head-on and grazing collisions. The results typically show that permanent coalescence (regime I) is favoured only for We smaller than a critical value which depends on the impact parameter. For larger values of We, the initially merged droplets would subsequently split apart, frequently with the simultaneous production of smaller satellite droplets. Furthermore, splitting is promoted when the collision is either near head-on or near grazing, as respectively designated by regimes IV and V in figure 1.

Recognizing that hydrocarbons are actually the relevant liquid for the study of spray combustion, and that their rheological properties can be quite different from those of water, Jiang, Umemura & Law (1992) conducted experiments on the collision of hydrocarbon droplets. A typical collision outcome, shown in figure 2, illustrates that the collisional dynamics of the hydrocarbon droplets can be significantly different from, and richer than, those of water droplets. Specifically, figure 2 shows that, in addition to regimes I, IV and V for the water droplets, two transition regimes, II and

III, are also present. As such, collision between the two hydrocarbon droplets does not always result in initial coalescence. Rather, as *We* is gradually increased from regime I, beyond a critical *We* the droplets will bounce apart upon collision without attaining any initial merging. This characterizes the behaviour of regime II. As *We* is further increased to that in regime III, coalescence upon collision is again possible. Only for sufficiently high *We* will regime IV, observed for water droplets, occur.

There are three distinctive aspects of the present investigation. First, subsequent to our previous study on droplet collision (Jiang *et al.* 1992), we became aware of the usefulness of the collision images reported therein in terms of their serving as benchmark simulation cases in the development of CFD methods, such as those of front-capturing and front-tracking, for the study of the dynamics of sharp interfaces separating fluids of significantly disparate densities (Chorin 1980; Boris 1989; Unverdi & Tryggvason 1992; Nobari & Tryggvason 1996). However, we also recognized that these previous images were not sufficiently time-resolved, and that some salient physics were either not captured or appreciated when we reported our earlier results. We have therefore significantly improved our imaging and data acquisition system, and consequently obtained detailed images of the droplet collision regimes (I)–(V).

The second aspect of the present contribution is that we have identified the importance of the displacement of the inter-droplet gaseous film in effecting droplet coalescence by demonstrating that there exist situations in which water droplets would exhibit the regimes II and III behaviour previously only observed for hydrocarbon droplets (figure 2), while the hydrocarbon droplets could also exhibit the collision responses of water droplets shown in figure 1. The apparently different droplet collision responses of water and hydrocarbons have therefore been unified. We shall provide extensive empirical evidence on the importance of the gas properties in controlling the bouncing and permanent coalescence outcomes of regimes I, II and III.

The third aspect of the study is concerned with the head-on transition between regimes III and IV. We have developed a phenomenological analysis for this transition and obtained a transition criterion which successfully correlated the experimental results.

The experimental apparatus adopted in the present study is that of Jiang *et al.* (1992), in which two identical streams of droplets of uniform and controlled size, produced by the ink-jet printing technique, impinged on each other. Time-resolved images were obtained through stroboscopy synchronized with the droplet generation circuit. The entire apparatus was housed in a chamber whose internal pressure could be varied between 0.1 and 20 atm. Vibrations in the laboratory were found to have no influence on the experimentation. Pure hydrocarbons and de-ionized water were used to produce droplets with diameters ranging from about 200 to 400 μm. The experiments were performed at room temperature and the collision phenomena observed were repeatable from run to run.

A video image software (Mediagrab) was used to grab the collision images from the video camera and store them for subsequent analysis of the instantaneous droplet size and velocity. This image acquisition system allows the fine resolution of the collision events and consequently the transition behaviour and boundaries between different regimes. In all the experimental collision images presented (figure 4), the stroboscope provided a uniform source of back lighting for the images. Thus areas of different shading indicate different amounts of light transmission through the colliding masses which act as optical lens in diffracting the light. This additional information may be useful in exploring the three-dimensional nature of the collision process through computational simulation.

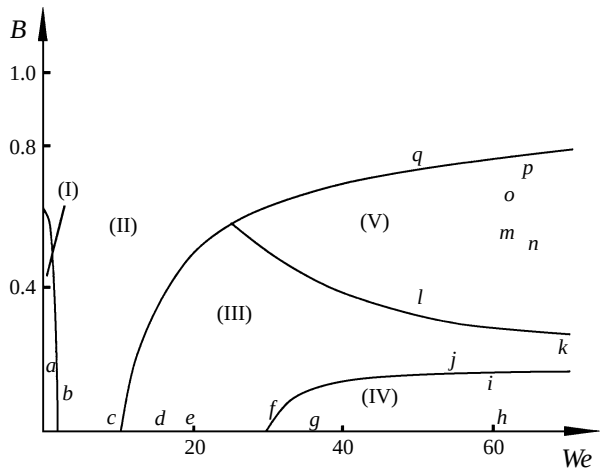

FIGURE 3. Locations of photographic collision images (*a*)–(*r*) in figure 4 in *We*, *B* coordinates.

Before presenting results from the three aspects of the study outlined above, it is useful to identify the controlling physical and dimensionless parameters for the present phenomena. Specifically, there are eight relevant physical parameters, namely U, R, χ, σ, and the densities and viscosity coefficients of the gas and the liquid. From these eight physical parameters, five dimensionless parameters can be formed, such as We, B, Re based on, say, the liquid density and viscosity, and the ratios of the densities and viscosity coefficients. Thus for a fixed liquid–gas system, the collision outcomes are defined by the three dimensionless groups of *We*, *B* and *Re*. Since the collisional dynamics and configuration are represented by *U*, *R* and χ, a phenomenological discussion of the various collision regimes, for a system of given rheological properties, can best be conducted by considering *We* (or *Re*) and *B*, as shown in figures 1 and 2.

2. Qualitative collision dynamics

Previous investigations (Park 1970; Ashgriz & Poo 1990; Jiang *et al.* 1992) showed droplet collision images but did not provide sufficient time resolution to delineate the intricacies of the collision dynamics. Our digital imaging system combined with synchronized droplet generation enabled us to observe and record the detailed droplet collision history in the various collision regimes with prescribed *We* and *B*. Of particular interest is the characterization of the transition between different collision regimes and the identification of the controlling mechanisms which affect the collision outcomes. We thus present in figure 4(*a–r*) the collision history of tetradecane droplets in 1 atm. nitrogen for regimes I–V. The letters (*a*)–(*r*) in the response plot of figure 3 correspond to the collision images in figure 4, indicating their respective values of *We* and *B*, which are also indicated in the figure caption together with the droplet radius *R*.

2.1. *Near head-on collisions*

Figure 4(*a*) shows a typical regime I collision which results in coalescence. It is seen that the two droplets experience very small deformation as they approach each other, with the maximum deformation attained at about 1.21 ms. The extent of deformation subsequently decreases, indicating that the droplets start to move away from each other. While it is not clear whether the droplets have connected at this stage, a

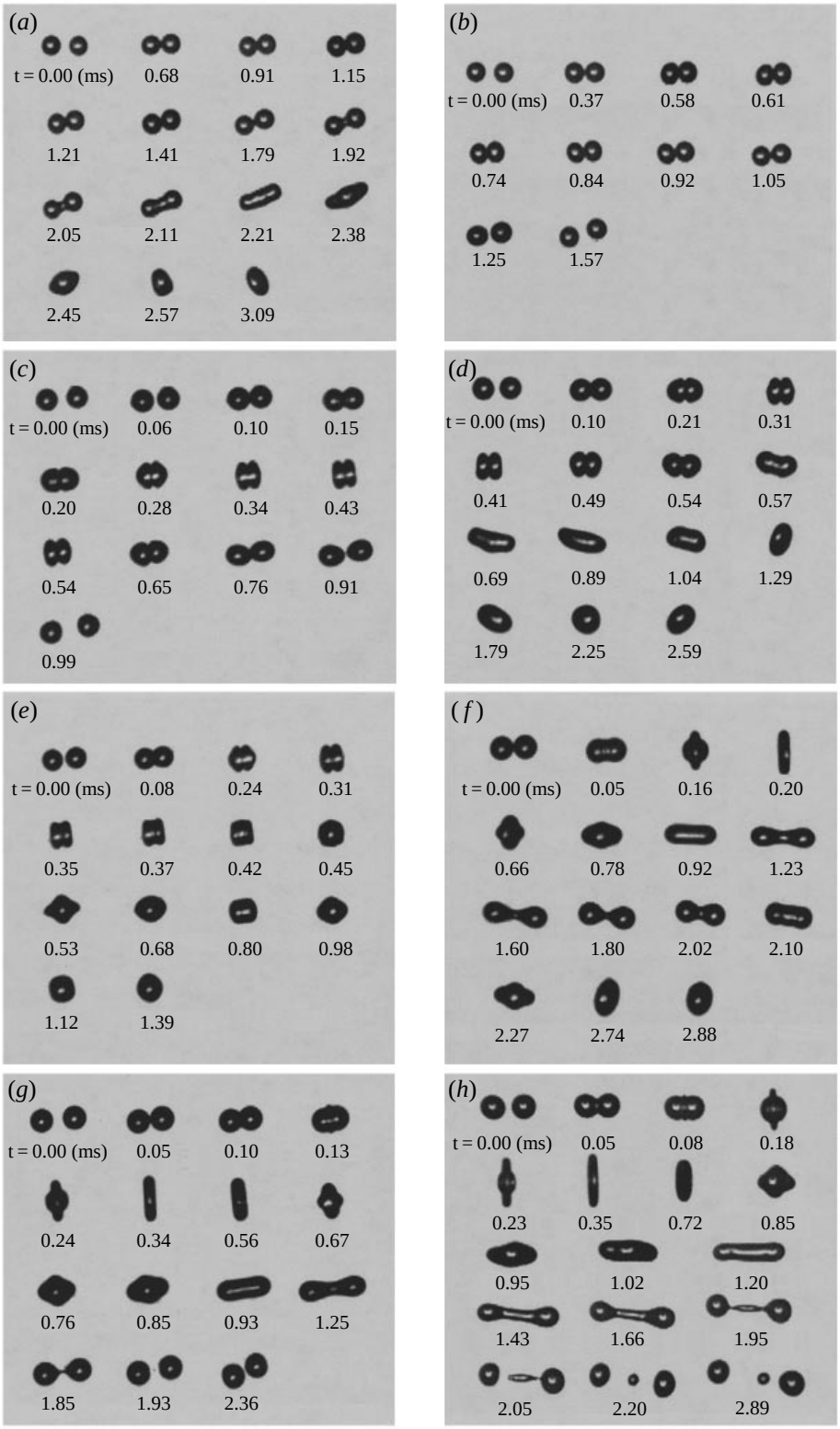

FIGURE 4(*a–h*). For caption see page 65.

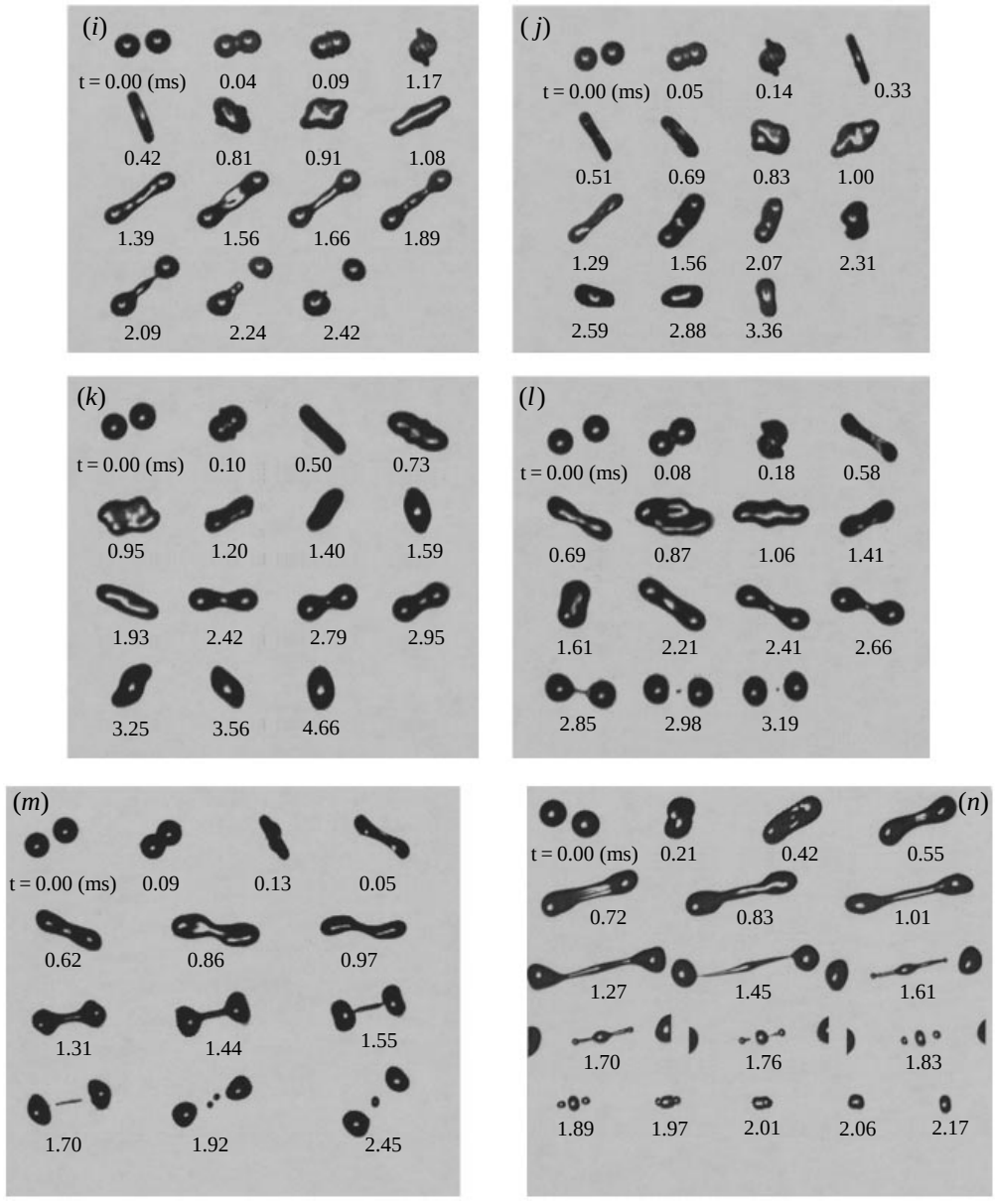

FIGURE 4(*i–n*). For caption see facing page.

connection does become evident at $t = 1.92$ ms, which eventually leads to the formation of a stretched liquid cylinder at about $t = 2.11$ ms. Surface tension then pulls the cylinder into a sphere, with basically no oscillation. The important point to note here is that the bulk of the droplets actually start to move away from each other either shortly before and certainly after coalescence has occurred.

With increasing relative velocity, figure 4(*b*) shows that the droplets bounce off without coalescence in regime II. The extent of droplet deformation is quite small because *We* is just slightly larger than the transition value from regime I. However, with increasing *We* figure 4(*c*) shows that the extent of droplet deformation assumes the same order as the droplet size, even though the droplets eventually still bounce

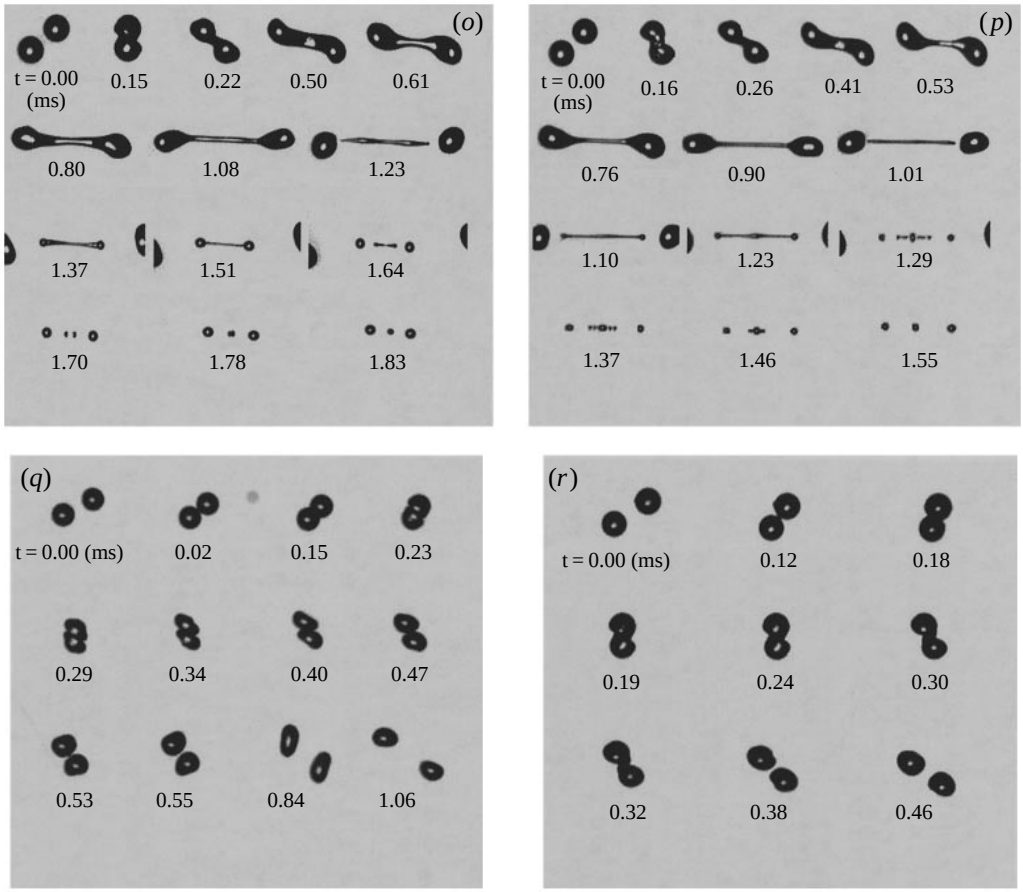

FIGURE 4. Photographic images showing representative collision sequences. (*a*) (*We*, *Re*, *B*, *R*) = (0.2, 14.8, 0.20, 120 μm); (*b*) (0.5, 23.6, 0.10, 131); (*c*) (8.6, 105.9, 0.08, 153); (*d*) (15.2, 139.8, 0.08, 151); (*e*) (19.4, 158.0, 0.05, 151); (*f*) (32.8, 210.8, 0.08, 159); (*g*) (37.2, 228.0, 0.01, 164); (*h*) (61.4, 296.5, 0.06, 168); I(*i*) (61.3, 295.3, 0.11, 167); (*j*) (56.3, 288.9, 0.13, 174); (*k*) (70.8, 327.7, 0.25, 178); (*l*) (48.1, 270.1, 0.39, 178); (*m*) (60.1, 302.8, 0.55, 179); (*n*) (65.1, 320.3, 0.49, 185); (*o*) (60.8, 313.7, 0.68, 190); (*p*) (64.9, 312.8, 0.71, 177); (*q*) (48.8, 260.3, 0.72, 163); (*r*) (14.5, 149.1, 0.34, 180).

away. The pointed shape of the droplets at $t = 0.65$ ms indicates the presence of outward motion in the droplet interior as the droplets bounce away from each other.

The above phenomena can be explained by recognizing that, in order for the droplets to coalesce, the gas between them must be squeezed out to such an extent that the inter-droplet gap is reduced to a dimension comparable to that of the molecular interaction, typically of the order of 10^2 Å (Mackay & Mason 1963). Thus, as the droplets approach each other, high pressure is built up in the gap, causing flattening of the droplets and conversion of the droplet kinetic energy into surface tension energy. The kinetic energy is also partly dissipated through the internal motion within the droplet and, to a much smaller extent, the gas flow inside the gap. Coalescence occurs when the minimum gap size reaches the molecular interaction range, while bouncing occurs when the minimum gap size is larger than this range. We therefore expect that the attainment of either coalescence or bouncing depends not only on *We*, but also on the properties of the gas as well as the surface tension and viscosity of the liquid.

The above discussion on the tendency for droplet coalescence assumes that, during

the collision time, a negligible amount of the gas in the inter-droplet gap is absorbed by the droplet. To demonstrate that this is indeed the case, we note that from Henry's law (Seinfeld 1986), $C = HC_g$, where C and C_g are the molar concentrations of the gaseous component in the surface layer of the liquid and within the gas gap, respectively, and H is the Henry coefficient which is of the order of 10^{-3} at room temperature. Thus the amount of gas absorbed in the liquid can be evaluated as $\delta RC\tau$, where τ is the collision time which is of the order of the droplet oscillation time, $(\rho R^3/\sigma)^{1/2}$, and δ is the gas diffusion coefficient which is typically of the order of $10^{-9}\ \mathrm{m^2\ s^{-1}}$. Therefore the fractional amount of the gas within the gap which is absorbed during collision can be estimated as $\delta RC\tau/R^2hC_g$, where h is the characteristic gap thickness which will be subsequently shown to be $(\rho_g R^3U^2/\sigma)^{1/2}$. Substituting the numerical values for the various parameters we find that this ratio is of the order of 10^{-6}, thereby demonstrating that the effect of gas absorption during collision is negligible.

Figure 4(*d*) shows droplet coalescence in regime III, close to the boundary between regimes II and III. We note that the image at 0.49 ms shows a cusp at the rim of contact, while the image at 0.54 ms shows a rounded profile. Similar configurations are also observed in figure 4(*e*) at 0.31 ms and 0.35 ms, respectively. Since the connection of the two surfaces is expected to rapidly smooth out the cusp at the rim, the brief period during which such a change of curvature occurs can be taken as the state of coalescence. We further note that the collisional inertia of the droplets in figure 4(*d*) is just high enough to allow for the viscous loss associated with droplet deformation and to overcome the resistance force of the gas film, rendering coalescence possible. The collision sequence is similar to that of figure 4(*a*) in that the connection between the droplets takes place as the droplet centres move away from each other. However, the droplets are significantly deformed in the present case. The coalesced droplet mass oscillates with a frequency of the order of 1 ms, which is of the same order of magnitude as that obtained by using $(\sigma/\rho R^3)^{1/2}$ based on dimensional reasoning.

Figures 4(*e*) and 4(*f*) further show sequences of the coalescence collision with larger We in regime III. It is seen that merging now appears to be accomplished as the droplets reach their largest deformation, without any indication of subsequent outward motion. This implies that for these high impact inertia situations the gap dimension quickly approaches that of the molecular force range as the droplets move towards each other. The collision sequence of figure 4(*f*) is close to the boundary of regime IV, in which separation after merging occurs. Consequently the merged mass for this state assumes the maximum amount of deformation. Specifically, the strong initial impact converts the kinetic energy into surface energy through the formation of a thin dimpled disk having a small radius of curvature at its edge. This disk subsequently contracts to form a cylinder, which then evolves into a dumb-bell because of the substantial amount of the outwardly directed axial internal motion. The outward motion, however, is not sufficient to split the merged mass apart. It therefore remains coalesced as the surface tension force pulls the end of the dumb-bell back.

Regime IV shown in figures 4(*g*) and 4(*h*) is entered with further increase in the impact energy. Figure 4(*g*) shows that the internal flow now has enough kinetic energy to overcome the surface tension force and break the connecting neck, leading to separation and the simultaneous formation of a tiny satellite droplet. The satellite droplet is formed when the connecting neck is pinched off as its two ends contract owing to spherodization of the incipient formation of the two separated droplets. This pinching action can also be seen clearly in figure 4(*h*), in which a larger satellite droplet is formed.

2.2. *Off-centre collision at high impact inertia*

We now discuss effects of the impact parameter B on bouncing and the tendency of the merged droplet mass to separate. Conceptually, for off-centre collisions, the normal component of the impact inertia can be considered to be mainly responsible in overcoming the gaseous film between the droplets. The tangential component is translated into a rotational motion of the merged mass.

We use the strong head-on collision sequence of figure 4(*h*) as the reference. Then with a slightly off-centre collision, figure 4(*i*) shows that the collision event is similar to that of figure 4(*h*), except for the presence of a rotational motion for the merged mass. With a further increase in B, figures 4(*j*) and 4(*k*) show that separation ceases to be possible and permanent coalescence results. Here, because of the reduced extent of the normal component of the impingement inertia, the component of the internal liquid motion responsible for separation is correspondingly reduced.

As B is further increased to that in regime V, separation after merging again becomes possible. Figure 4(*l*) represents such a sequence just beyond the transition boundary from regime III, and shows that, at $t = 1.61$ ms, the two droplets have completely merged into a large rotating mass. It is seen that this liquid has already rotated 180° at $t = 2.21$ ms. However, the stronger centrifugal force now causes the merged mass to stretch and eventually break up. This breakup corresponds to the phenomenological analysis of Brazier-Smith *et al.* (1972), which states that breakup is possible when the rotational kinetic energy exceeds the surface tension energy required to maintain the merged droplet as a single mass. However, since liquid-phase viscous dissipation is substantial for droplet collision, as demonstrated in our previous study (Jiang *et al.* 1992), their inviscid analysis is not quantitatively descriptive of the collision event. We further note that since separation occurs after merging, with rotational motion being an important element responsible for the separation, the analyses of Park (1970) and Ashgriz & Poo (1990), based on the intensity of shearing through a small contact area of the two droplets, are not consistent with the observation.

Figures 4(*m*)–4(*p*) show the collision sequences with high We and B, which are characterized by the formation of multiple satellite droplets and which will be discussed in the next section. For sufficiently large B, the normal component of the impact inertia is substantially reduced such that collision exhibits the bouncing behaviour of regime II, as shown in figure 4(*q*). Thus figures 4(*h*)–4(*q*) demonstrate the high-We collision behaviour from near head-on separation (IV), to coalescence (III), to off-centre separation (V), and finally to bouncing (II), as the collision orientation changes gradually from head-on to highly off-centre.

For the sake of completeness, we also show the off-centre bouncing collision at a medium Weber number (figure 4*r*). Compared with figure 4(*q*), here the two droplets do not form disks during bouncing collision.

2.3. *Formation of satellite droplets*

The separation process in regimes (IV) and (V) is characterized by the formation and the subsequent 'pinch off' of a connecting ligament as the two main droplet masses move away from each other. This ligament can then either contract to form a single droplet, as in figure 4(*l*), or further break up into more satellite droplets, frequently in a cascading manner. To demonstrate the richness of the phenomenon of multiple satellite droplet formation, we first note from figure 4(*m*) that two equal sized satellites are produced as the ligament breaks up in the middle. These two satellite droplets subsequently approach each other and coalesce into a single droplet. For larger values

of *We* and *B*, a longer stretched ligament is produced and the number of satellite droplets which subsequently form also increases. For example, figure 4(*n*) shows that two satellite droplets are further pinched off from the ends of the ligament, with the remaining ligament contracting to form a third satellite of larger size, while figures 4(*o*) and 4(*p*) show further pinching off of end satellites from the remaining segment. Specifically, a total of seven droplets are produced at $t = 1.37$ ms in figure 4(*p*). It is also significant to note that, except for the two parent droplets, which move away from each other, all the satellite droplets actually move towards the centre of the ligament and some of them subsequently recombine.

The mechanism of ligament breakup and satellite droplet formation observed herein is that of the 'end-pinching' mechanism proposed and established by Leal and co-workers (Stone, Bentley & Leal 1986; Stone & Leal 1989) through experimental and computational studies. Figure 5 shows a schematic of such a process for a half ligament. Here, we first note that when the stretched liquid ligament separates from the main droplets, a non-uniform pressure field is set up within the ligament. Specifically, the curvature in the radial and lateral directions causes the pressure in the ligament to be higher than that of the ambient owing to surface tension effects. Furthermore, the rounded end possesses an additional curvature, as compared to the cylindrical segment, making the internal pressure there higher than that in the midsection. The resulting pressure differential then generates a local flow which pulls the rounded end towards the midsection, as indicated in figure 5(*b*). Such a motion causes the end to become bulbous because of mass accumulation. This change in surface geometry implies that there is a negative curvature and hence a location of pressure minimum between the bulbous end and the midsection, and consequently induces a local flow towards the end through this minimum pressure point, as shown in figure 5(*c*). The motion causes a local reduction in the mass and hence a neck is formed. The formation of this neck elevates the pressure there because of the reduction of the local ligament radius, which consequently induces an additional motion from the neck towards the midsection and leads to a further reduction of the radius of the neck, as shown schematically in figure 5(*d*). The situation is clearly unstable, leading to a rapid shrinkage of the neck and eventual pinching off of the bulbous end. The 'end-pinching' motion leaves a cylindrical thread of liquid, which either relaxes to form a single satellite as shown in figure 4(*n*), or continues to pinch off more satellites as seen in figures 4(*o*) and 4(*p*).

It is of interest to note the remarkable similarity between the present satellite droplet formation processes and images and those of Stone *et al*. (1986) in which the ligament was independently produced through pinching instead of capillary wave instability. Stone & Leal (1989) also numerically showed that capillary wave instability was in effect only for ligaments with high elongation ratios, far exceeding those of the ligaments produced in the present droplet collision experiments. Furthermore, Frankel & Weihs (1987) showed that viscous effect can damp and delay the development of the capillary wave disturbances. These results, together with our additional observation that the coalesced ligament does not simultaneously break up into uniform satellites, provides strong evidence that satellite droplet production in droplet collision is through the action of pinching instead of capillary-wave instability.

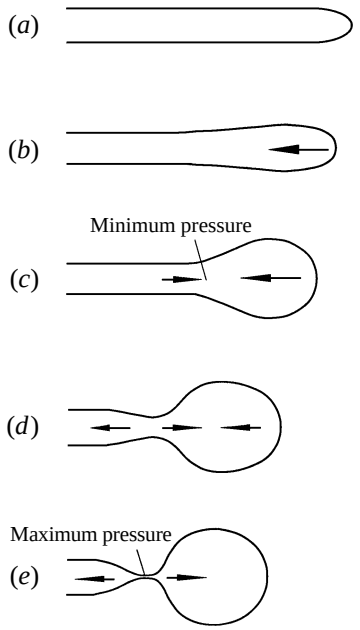

FIGURE 5. Schematic of the ligament 'end-pinching' mechanism.

3. Transitions between regimes I, II and III

3.1. *Phenomenological considerations*

Figures 4(*a*)–4(*r*) are typical of hydrocarbon droplet collision at 1 atm. air or nitrogen. However, as noted previously (Jiang *et al.* 1992), the bouncing regime II is absent for water droplets such that regimes I and III merge. In order to experimentally investigate the various factors which could affect the transitions from regimes I to II to III in general, and thereby explain the qualitatively different collision response between water and hydrocarbon droplets in particular, it is necessary to first identify the fundamental physical processes which control the coalescence and bouncing of the colliding droplets. As discussed earlier, coalescence may not occur readily when the droplets collide because of the presence of a gaseous film between the droplet interfaces that needs to be 'squeezed out', or 'discharged', before contact can be made. The resistance with which this inter-droplet film can be discharged then depends on the collision inertia of the droplets and the dynamics of the film flow including the pressure buildup within it. Conceptually, one would expect that complete discharge is favoured either for a sufficiently slow rate of approach (regime I) such that there is ample time for discharge, or for a sufficiently high rate of approach (regime III) such that discharge is forcibly accomplished. Consequently, it is reasonable to expect that there should exist a regime II, for moderate rates of approach, for which the discharge is not accomplished. For such situations the colliding droplets lose all their impact inertia before contact, as a consequence of the substantial pressure buildup in the inter-droplet region as well as the conversion of part of the kinetic energy to surface energy through droplet deformation and the dissipation of the rest of it through viscous action. The deformed droplet masses subsequently bounce away as they attempt to restore their spherical shape through surface tension. Furthermore, in regime I the pressure rise in the inter-droplet region and hence the droplet deformation should be small such that the minimum clearance distance occurs on the line of centres of the colliding droplets. However, in regime III a high-pressure field is build up in the direction of the line of

centres, resulting in indentations on the droplet surfaces in this region and substantial flattening of the droplets. The minimum clearance then assumes the form of a ring concentric with the line of centres, a discussed previously (Lee & Hodgson 1968; Jiang *et al*. 1992).

Except for low *We* situations, substantial droplet deformation occurs during the collision. The initial flattening of the droplets absorbs the impact kinetic energy and converts it to surface energy, while the subsequent restoration converts it back. The deformation and restoration are necessarily associated with substantial internal motion within the droplets, and could result in a fair amount of dissipative loss as shown in Jiang *et al*. (1992). Furthermore, the flattening increases the impact surface area and consequently the total repulsive force experienced by the droplets. We also note that the motion of the gas film and that within the droplet are intimately coupled through the no-slip boundary condition before the gap reaches the molecular force range. Thus, a highly viscous droplet fluid would induce more viscous resistance and hence a greater difficulty to discharge the gas film.

The final consideration is the factor controlling the actual merging of the surfaces. Mackay & Mason (1963) showed that the colliding droplets may coalesce when their clearance reaches a critical value which is within the range of the intermolecular forces of the droplet fluid, typically of the order of 10^2 Å. Therefore, the parameters characterizing the intermolecular forces between the droplet and gas fluids in general, and the molecular structures of these fluids in particular, are expected to be of relevance also.

Based on the above considerations, we can now link the following properties of the liquid/gas system to the droplet collision response and hence transition. The first, and perhaps most important property should be the gas density since it directly affects the inertia of the gas film. Furthermore, the gas viscosity should also be important because it describes the viscous loss associated with the low-Reynolds-number flow of the thin gas film. For the droplet fluid properties, we would expect that the surface tension and viscosity are the relevant parameters. Finally, the intermolecular force parameters, as well as the similarity and dissimilarity of the molecular structures of the droplet fluid and gas, should control the tendency for the final merging of the droplet surfaces. This last set of molecular parameters was not included in our initial consideration of the controlling physical parameters for the present phenomena, as discussed toward the end of §1.

Since the surface tension forces and the viscosities of water and hydrocarbon are quite different, it is reasonable to expect that their collision behaviour can also be quite different. Since bouncing collision is not observed or water, at 1 atm. air, it can be conjectured that this is because of the higher surface tension and lower viscosity of water compared to those of the hydrocarbons. The relatively small surface deformation and viscous dissipation energy therefore facilitate coalescence. On the other hand, since the collision outcome also depends on the gas properties, it may also be conjectured that through judicious variation of the gas-phase parameters, their behaviour can be described through a unified viewpoint.

The experimental investigation reported here was guided by the above reasoning and subsequently substantiated it. The results will be presented in terms of the collision regimes in the *We*, *B* space. A unified quantitative correlation of the transition boundaries has not been achieved because of the large number of parameters and the lack of a comprehensive theory. The experimental results are, however, interesting and significant in their own right, providing quantitative data and useful insights for further theoretical exploration and computational simulation.

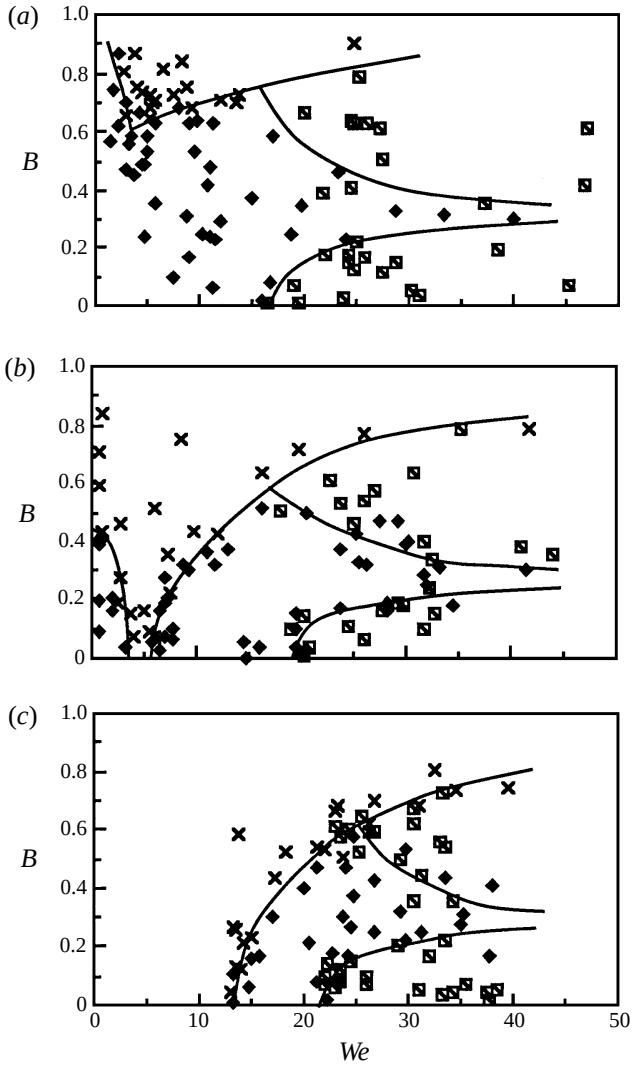

FIGURE 6. The transition of water droplet collision regimes versus pressure in the nitrogen environment. ◆, coalescence; ×, bouncing; ⧅, separation. (*a*) 1 atm. (*b*) 2.7 atm. (*c*) 8 atm.

3.2. *Effects of gas pressure*

Since the inertia of the gas film is directly affected by its density, a straightforward approach to explore this effect is to vary the gas pressure. Figures 6 and 7, respectively, show the collision regimes for water and *n*-tetradecane (n-$C_{14}H_{30}$) in nitrogen environments of different pressures.

We first note that in order to promote the occurence of bouncing for water droplets, which has not been previously observed in 1 atm. air, we should increase the gas density; note that the viscosity of the gas remains fairly constant with increasing density for the pressure range investigated herein. In the course of the experimental exploration, we have found that water droplets actually do exhibit the bouncing phenomenon in 1 atm. air (or nitrogen as in the present experiments), albeit at high values of B, as shown in figure 6(*a*). This regime apparently was mostly overlooked, and was only briefly mentioned in Park (1970). We have subsequently found that, with

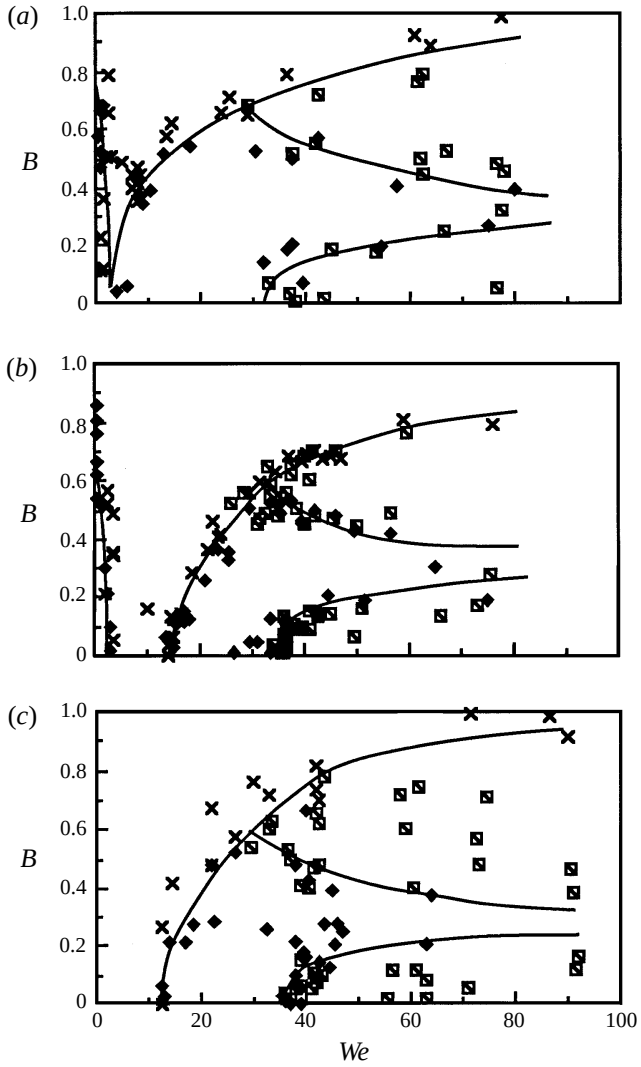

FIGURE 7. The transition of tetradecane droplet collision regimes versus pressure in the nitrogen environment. ◆, coalescence; ×, bouncing; ⧅, separation. (*a*) 0.6 atm. (*b*) 1 atm. (*c*) 2.4 atm.

increasing pressure, this regime expands and moves to include small values of B as shown in figures 6(*b*) and 6(*c*). When the pressure is increased to around 2.7 atm., a fully-developed regime II is observed, in that droplet bouncing now occurs for both off-centre and head-on collisions. We have therefore demonstrated that the five collision regimes for hydrocarbons also exist for water, at elevated pressures.

Recognizing that increasing pressure promotes bouncing, it is then reasonable to expect that decreasing pressure should suppress bouncing. Figures 7(*a*) and 7(*b*) for the tetradecane droplets show that this is indeed the case in that, while the five regime response is observed at 1 atm., the head-on bouncing regime is suppressed as the pressure is reduced to 0.6 atm. Experimentation at lower pressures was not successful owing to instabilities in droplet generation. One potential cause of the instabilities is the onset of cavitation in the flow circuit under reduced pressure.

We have further found that, by increasing the nitrogen pressure to 8 atm. for water

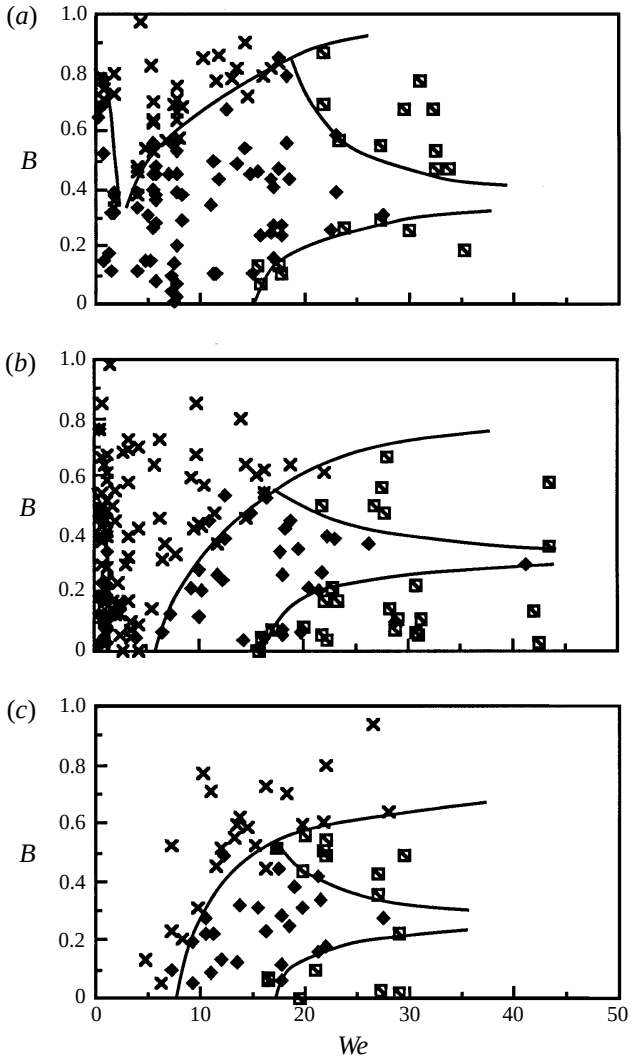

FIGURE 8. The transition of water droplet collision regimes versus pressure in the helium environment. ◆, coalescence; ×, bouncing; ⧅, separation. (*a*) 4.4 atm. (*b*) 7.5 atm. (*c*) 11.7 atm.

droplets and 2.4 atm. for tetradecane droplets (as shown in figures 6(*c*) and 7(*c*)) regime II can be expanded to such an extent that regime I cannot be experimentally detected. Realistically, of course, two droplets will merge when they are slowly brought together. We have, however, not been able to simulate such a slow rate of collision in our experiments. The important point to note is that low-*We* head-on collision at high pressures could very probably result in bouncing. This is to be contrasted with the previous concept, based on water at 1 atm., that low-*We* head-on collision always results in coalescence.

3.3. *Effects of gas molecular weight and viscosity*

To further demonstrate the influence of the inertia of the gas film through its density, additional experiments have been conducted for the 'lighter' helium environment. The collision response regimes for both water and tetradecane are shown in figures 8 and 9. The results clearly show that, because of the reduced molecular weight and hence

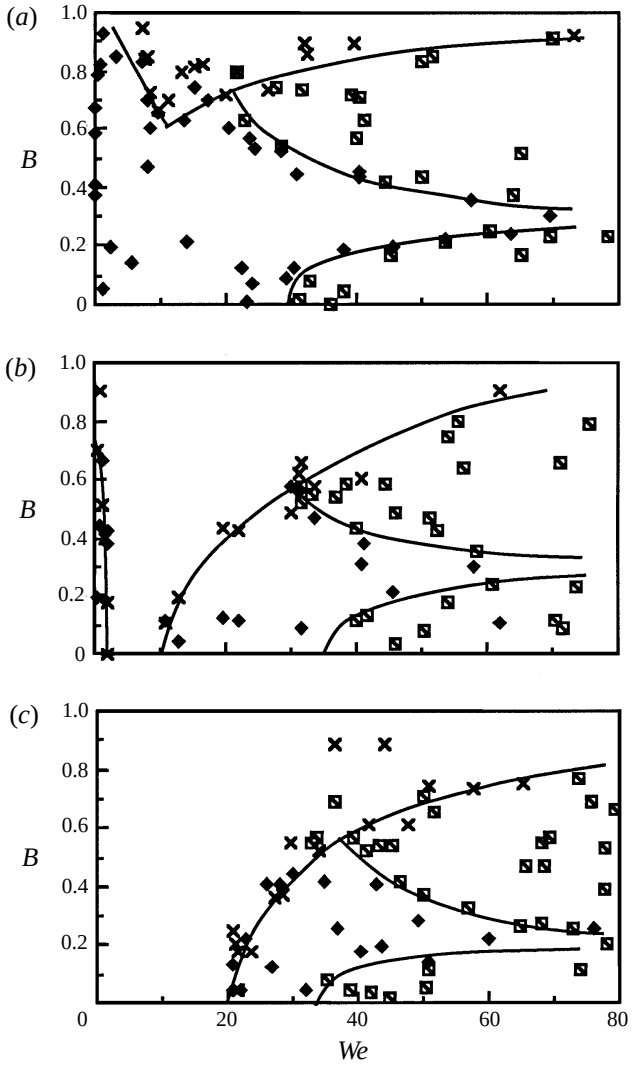

FIGURE 9. The transition of tetradecane droplet collision regimes versus pressure in the helium environment. ◆, coalescence; ×, bouncing; ⧅, separation. (*a*) 0.7 atm. (*b*) 2.4 atm. (*c*) 4.4 atm.

density of the helium atmosphere, a higher pressure is needed to induce bouncing in regime II and suppress coalescence in regimes I and III.

Gas density, however, is not the only parameter influencing the collision outcome. To demonstrate this point, we note that while the gas density for 1 atm. nitrogen in figure 6(*a*) is almost the same as that for 7.5 atm. helium in figure 8(*b*), bouncing is clearly more prominent for the helium atmosphere. This difference is believed to be caused by the higher viscosity of helium, 194 μP versus 174 μP at 20 °C, such that the gas film cannot be discharged sufficiently fast. This consequently leads to a higher pressure buildup within the gap and a stronger propensity for bouncing. More study, however, is needed to clearly identify the role of gas viscosity in bouncing.

We next note that since inertia and viscous forces are both important in affecting the droplet collision outcome in this phenomenon, it is reasonable to expect that the characteristic Reynolds number for the gas flow inside the gap is of order unity. To

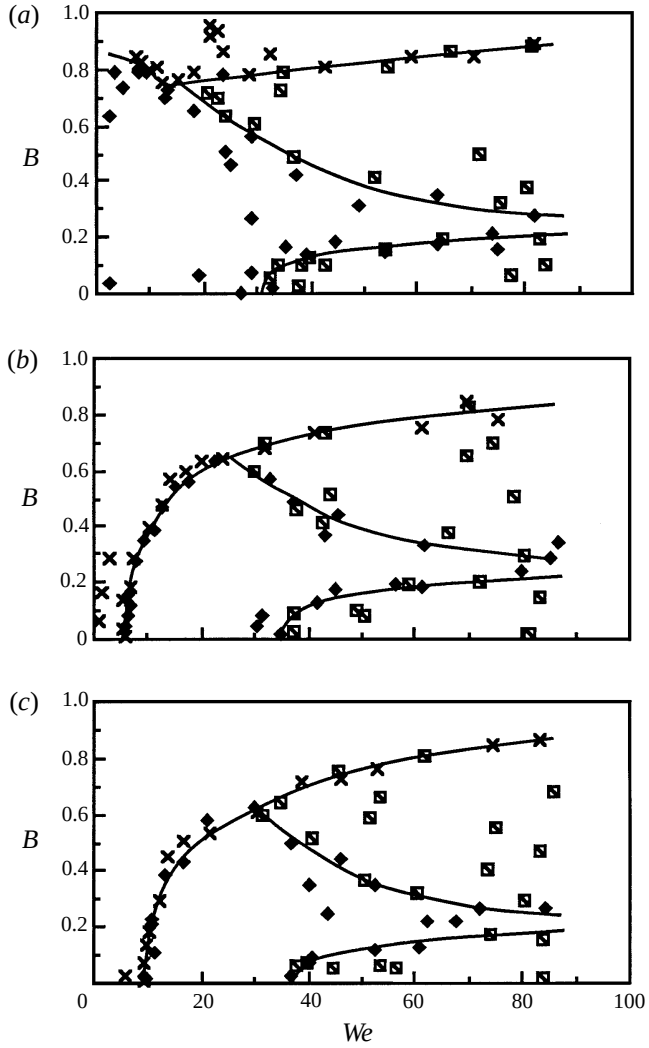

FIGURE 10. The transition of tetradecane droplet collision regimes in 8 atm. ethylene–nitrogen environment. ◆, coalescence; ×, bouncing; ⧅, separation. (*a*) 100% ethylene. (*b*) 50% ethylene – 50% nitrogen. (*c*) 100% nitrogen.

demonstrate this feature, we note that the characteristic transverse velocity u of the gas in the gap is of order UR/h, while the dynamic pressure inside the gap, $\frac{1}{2}\rho_g u^2$, which results in the deformation of droplet surface, is balanced by surface tension $2\sigma/R$. Therefore h is estimated as $(\rho_g R^3 U^2/\sigma)^{1/2}$ and the characteristic Reynolds number for the gap gas flow, $Re_h = \rho_g Uh/\mu_g$, is of the order of $(U^2\rho_g R/\mu_g)(\rho_g R/\sigma)^{1/2}$, where μ_g is the gas viscosity. Using representative experimental values, it is found that Re_h is indeed of order unity, implying that both the inertial and viscous forces should be included in computational simulations.

3.4. *Effects of gas molecular structure*

The nitrogen and helium environments used in the above studies are gases whose molecular structures are very different from either water or tetradecane. Furthermore, their solubility in these liquids are also very low. A spray interior, however, invariably

consists of some vapour of the droplet fluid owing to vaporization. Thus, to investigate the effects of fluid vapour, we have conducted tetradecane droplet collision experiments in environments of mixtures of nitrogen and ethylene (C_2H_4); ethylene is used because it has the same molecular weight as nitrogen and is structurally similar to tetradecane, both being aliphatic compounds. It is not possible to use tetradecane vapour as the gaseous environment because of its very low vapour pressure at room temperature.

Figure 10(*a*) shows the collision regimes of tetradecane droplet in pure ethylene at 8 atm. pressure. It is seen that the propensity to bounce is greatly reduced and only off-centre bouncing is observed. The bouncing tendency is improved when ethylene is diluted by nitrogen such that the head-on bouncing regime occurs for the 50–50 % case, as shown in figure 10(*b*). In particular, when the ambient environment is restored to pure nitrogen, bouncing for the head-on collision is fully restored as shown in figure 10(*c*).

We have therefore obtained the important result that the presence of fuel vapour in the interior of fuel sprays promotes coalescence. A similar observation can be made regarding the need to study water droplet collision in humid instead of dry environments for its relevance in rain-drop formation. The actual mechanism through which the presence of the fluid vapour (or a molecularly similar gas) can promote droplet coalescence is as yet unclear. It is possible that the presence of the vapour modifies the surface tension which in turn promotes droplet merging.

4. Criterion for head-on transition between regimes III and IV

The photographic images of figures 4(*f*)–4(*h*) show that upon near-head-on coalescence in regimes III and IV, the merged mass first assumes the shape of a dimpled disk having a small radius of curvature at its edge. This is the stage of the largest deformation and it was shown in Jiang *et al*. (1992) that the process of this deformation is accompanied by viscous dissipation. In particular, for water and the hydrocarbon droplets studied, about half of the initial kinetic energy is dissipated during this period. The disk subsequently contracts to form a cylinder, which then evolves into a dumb-bell because of the substantial amount of outwardly directed internal motion. If this outward motion is not sufficient to split the merged mass apart, then surface tension will pull the ends of the dumb-bell back. The excess energy is quickly dissipated within one cycle of oscillation. However, if the outwardly directed motion is sufficiently large, then splitting will take place. Figure 11 shows a simplified schematic of the process described above.

A phenomenological criterion was proposed by Ashgriz & Poo (1990) to describe the transition between near head-on coalescence and separation. The analysis considers the development of disturbance over the stretched liquid cylinder surface subsequent to coalescence, and yields the result that cylinder breakup is expected to occur when the length-to-diameter ratio of the cylinder exceeds π. Since the analysis is based on inviscid flow assumption, the phenomenon is characterized by a single parameter, namely *We*. In particular, the transition *We* between regimes III and IV, say We_c, was predicted to be around 19, which agrees well with the experimental data on water.

An examination of the present data, however, shows that We_c is 34 for tetradecane. Furthermore, the experimental results of Jiang *et al*. (1992) showed that We_c increases as the liquid viscosity increases. Finally, and perhaps most importantly, the capillary-wave instability mechanism for the breakup as proposed by Ashgriz & Poo (1990) is in variance with the experimental observation that separation of the coalesced mass is due to the strong internal liquid motion which overcomes both viscous dissipation and

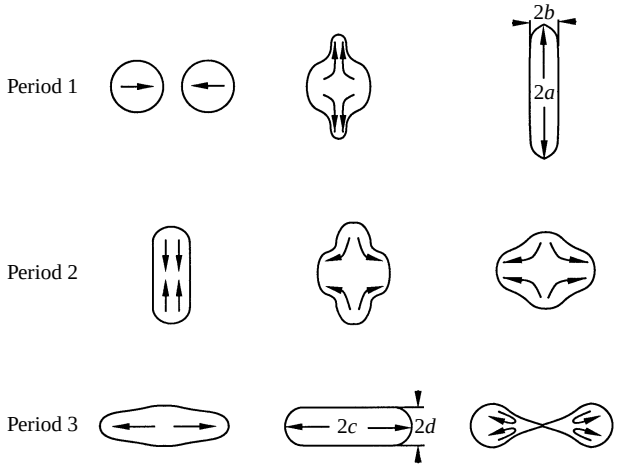

FIGURE 11. Schematic of the three periods of droplet separation collision sequence.

the surface tension force. Indeed, Stone & Leal (1989) showed that, if capillary-wave instability were the breakup mechanisms, then an extremely long cylinder would be required for the disturbance to develop, which is not what was observed experimentally.

In light of the above discussions, in this section we shall provide a phenomenological analysis for the breakup criterion based on considerations of the kinetic energy of the internal fluid motion, the surface tension energy of the liquid masses, and viscous dissipation. An expression for We_c is derived which agrees well with the experimental results for different liquids.

The droplet collision sequence that results in separation is divided into three periods shown schematically in figure 11. In period 1, two droplets first impinge head on and form an outwardly spreading disk. In period 2, the disk contracts under surface tension to recover the droplet shape, and the internal fluid moves inward in the manner of a counterflow. Finally, in period 3, a stretched liquid cylinder is formed, with its two ends moving outward and hence producing a thin inter-connecting ligament which eventually breaks.

At the critical transition from coalescence to separation, the initial kinetic energy is just large enough to overcome the viscous dissipation after coalescence and break the ligament. We can therefore write

$$E = \Phi_1 + \Phi_2 + \Phi_3 + \Phi_r, \tag{1}$$

where E is the initial kinetic energy given by $\frac{4}{3}\pi R^3\rho(\frac{1}{2}U)^2$. Here Φ_1, Φ_2 and Φ_3 are the dissipative losses during periods 1, 2 and 3. It may be noted that in writing 1 we have neglected the surface energy associated with the small satellite droplets produced during separation. Furthermore, we note that at the instant of breakup the droplet masses are highly deformed, hence possessing an additional surface tension energy, Φ_r, as compared to those of the original spherical droplets. This extra residual energy will be partly dissipated as the separated masses regain their spherical shape, with the rest converted to kinetic energy for the separated droplets as they move away from each other. It can be expressed as

$$\Phi_r = \Delta S\sigma \tag{2}$$

where ΔS is the additional surface area associated with the deformed shape.

The viscous dissipation during periods 1, 2 and 3 can be evaluated for the individual periods from

$$\Phi_{1,2,3} = \mu \int\int \frac{1}{2}\left(\frac{\partial v_i}{\partial x_j} + \frac{\partial v_j}{\partial x_i}\right)^2 \mathrm{d}t\,\mathrm{d}x^3. \tag{3}$$

The loss during period 1, Φ_1, has already been evaluated by Jiang *et al.* (1992) as

$$\Phi_1 = \tfrac{1}{6}\alpha\pi R^2\sigma We, \tag{4}$$

where α is the fractional amount of the initial energy dissipated. It is of interest to note that, because the characteristic velocity gradient and the dissipative volume themselves are related to the dissipative process, the dissipative loss in this period turns out to be independent of the viscosity coefficient of the fluid. For the water and hydrocarbon data (Jiang *et al.* 1992), α has been empirically determined to be around 0.5.

To evaluate Φ_2, we note that the characteristic liquid velocity v_2 towards the centre is evaluated from balancing the pressure and surface tension forces

$$\tfrac{1}{2}\rho v_2^2 = \sigma\left(\frac{1}{b} + \frac{1}{a}\right). \tag{5}$$

The time which lapses until the droplet recovers its quasi-sphere shape is a/v_2 and the volume is $\frac{8}{3}\pi R^3$. Consequently Φ_2 can be evaluated as

$$\Phi_2 \sim \tfrac{1}{2}\mu\left(\frac{v_2}{b}\right)^2\left(\frac{a}{v_2}\right)\tfrac{8}{3}\pi R^3 = \tfrac{4}{3}\pi R^{3/2}\mu\frac{\tilde{a}}{\tilde{b}^{5/2}}\left(\frac{2\sigma}{\rho}\left(1+\frac{\tilde{b}}{\tilde{a}}\right)\right)^{1/2} \tag{6}$$

where $\tilde{a} = a/R$ and $\tilde{b} = b/R$.

The viscous dissipation Φ_3 in period 3 is similarly evaluated as

$$\Phi_3 \sim \tfrac{4}{3}\mu\frac{cv_3}{d^2}\pi R^3 = \tfrac{4}{3}\pi R^{3/2}\mu\left(\frac{4\sigma}{\rho}\right)^{1/2}\left(\frac{\tilde{c}}{\tilde{d}^{5/2}}\right), \tag{7}$$

where

$$v_3 = \left(\frac{4\sigma}{\rho d}\right)^{1/2} \tag{8}$$

and $\tilde{c} = c/R$ and $\tilde{d} = d/R$.

Substituting all the Φ into (1), and normalizing the resulting expression by the initial surface energy $\sigma(8\pi R^2)$, we obtain

$$We_c = \beta Z + \gamma, \tag{9}$$

where $Z = 16\mu/(\rho R\sigma)^{1/2}$ is the Ohnesorge number, representing the ratio of the viscous to surface energies, the parameter β is defined as

$$\beta = \frac{1}{(1-\alpha)}\left[\frac{\tilde{a}}{\tilde{b}^{5/2}}\left(\frac{1}{2}\left(1+\frac{\tilde{b}}{\tilde{a}}\right)\right)^{1/2} + \frac{\tilde{c}}{\tilde{d}^{5/2}}\right], \tag{10}$$

$$\gamma = \frac{6\Delta S}{(1-\alpha)\,\pi R^2}. \tag{11}$$

The parameter β is a geometry parameter independent of the liquid properties at transition from coalescence to separation, and γ comes from the extra surface tension energy due to the deformed droplet surface (ΔS). Equation (9) indicates that the initial kinetic energy can be divided into two parts for the breakup of the coalesced liquid, namely the amount needed to overcome viscous dissipation through the internal liquid

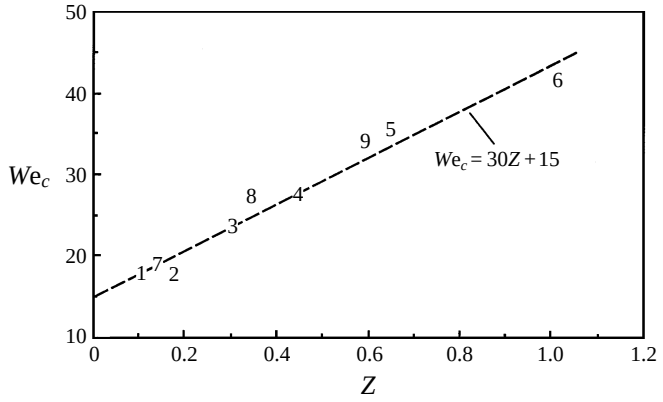

FIGURE 12. Critical Weber number (We_c) versus Ohnesorge number (Z) for separation collision in air or nitrogen environment. Park: 1, 2, water in 1 atm. N_2. Jiang *et al.*: 3, decane; 4, dodecane; 5, tetradecane; 6, hexadecane, all in 1 atm. air. Present: 7, water in 8 atm. N_2; 8, undecane in 1 atm. air; 9, tetradecane in 2.4 atm. N_2. Correlation: ———.

movement, as indicated by the Ohnesorge number Z, and the amount required to achieve the final deformed liquid shape as indicated by γ. Since there are five independent dimensional parameters given by ρ, μ, σ, U and R, we indeed need only two non-dimensional numbers to define the criterion for the transition from coalescence to separation.

Figure 12 shows the critical Weber number (We_c) versus Ohnesorge number (Z) for the experimental data (indicated by numerals) of Park (1970), Jiang *et al.* (1992), and the present investigation. The plot yields $\beta = 30$ and $\gamma = 15$. An independent evaluation of (10) from the measured values of $\tilde{a}$, $\tilde{b}$, $\tilde{c}$ and $\tilde{d}$ through deformed droplet shape images at critical transition for different liquids and at different pressures yields an average β of 24 ± 3. Furthermore, evaluating γ from the measured values of the surface area of the deformed droplet by assuming that it is a body of revolution, equation (11) yields an average γ of 10 ± 2. These independently evaluated values of β and γ therefore agree well with those determined from figure 12. The $Z = 0$ intercept of the correlation also indicates that for liquids with very small viscosity, the minimum required We_c for separation is given by the value of γ.

5. Concluding remarks

The present investigation presents a detailed description of the droplet collision dynamics based on a series of time-resolved images of the collision event with different collision inertia and impact parameter. Characteristics of different collision events in the five collision regimes are well represented by these time-resolved images. We have demonstrated that the previously observed difference in the collision behaviour for water and hydrocarbon droplets are consequences of their different viscosity and surface tensions, that the gas density has dominant influence on the potential of droplet merging upon collision, that droplet bouncing is promoted by increasing the pressure and molecular weight of the environment gas, and that the collision dynamics of water and the hydrocarbons are therefore fundamentally similar. The similarity and dissimilarity of the liquid and gas molecular structure can also critically influence the tendency of merging, implying that the presence of fuel vapour in the interior of fuel sprays may promote coalescence. We have also demonstrated that satellite droplet

production for high-inertia collisions is the consequence of ligament pinching instead of capillary-wave instability. Finally, a criterion governing the coalescence and separation of droplets for high Weber number, near head-on collisions, allowing for viscous dissipation, is derived and found to agree well with the experimental data.

Further studies are needed for the comprehensive understanding and description of droplet collision. Issues of particular interest are a criterion governing the transitions from regimes I, to II, to III, empirical/analytical descriptions of the extents of droplet deformation and internal viscous loss and of the production of satellite droplets, and the phenomena of off-centre collision in general. Computational simulation is currently in progress to enhance the physical understanding, especially the dynamics of the inter-droplet gas motion which cannot be readily studied experimentally.

This research was supported by the Air Force Office of Scientific Research under the technical monitoring of Dr Mitat Birkan. We thank T. G. Kreutz, D. L. Zhu and X. Zhu for their assistance in the course of this investigation.

REFERENCES

Adam, J. R. & Lindblad, N. R. 1968 The collision, coalescence, and disruption of water droplets. *J. Appl. Phys.* **39**, 173.

Ashgriz, N. & Poo, J. Y. 1990 Coalescence and separation in binary collision of liquid drops. *J. Fluid Mech.* **221**, 183.

Boris, J. P. 1989 New direction in computational fluid dynamics. *Ann. Rev. Fluid Mech.* **105**, 61.

Brazier-Smith, P. R., Jennings, S. G. & Latham, J. 1972 The interaction of falling water drops: coalescence. *Proc. R. Soc. Lond.* A **326**, 393.

Chorin, A. J. 1980 Flame advection and propagation algorithms. *J. Comput. Phys.* **35**, 1.

Faeth, G. M. 1977 Current status of droplet and liquid combustion. *Proc. Energy Combust. Sci.* **3**, 191.

Frankel, I. & Weihs, D. 1987 Influence of viscosity on the capillary instability of a stretching jet. *J. Fluid Mech.* **185**, 361.

Jiang, Y. J., Umemura, A. & Law, C. K. 1992 An experimental investigation on the collision behaviour of hydrocarbon droplets. *J. Fluid Mech.* **234**, 171.

Lee, J. C. & Hodgson, T. D. 1968 Film flow and coalescence – I, basis relations, film shape and criteria for interface mobility. *Chem. Engng Sci.* **23**, 1375.

Mackay, G. D. & Mason, S. G. 1963 The gravity approach and coalescence of fluid drops at liquid interfaces. *Can. J. Chem. Engng* **41**, 203.

Nobari, M. R. H. & Tryggvason, G. 1996 Numerical simulations of three dimensional drop collisions. *AIAA J.* **34**, 750.

O'Rourke, P. J. & Bracco, F. V. 1980 Modeling of droplet interactions in thick sprays and a comparison with experiments. *Stratified Charge Auto. Engng Conf., Mech. Engng Pub.* ISBN 082984693.

Park, R. W. 1970 Behavior of water drops colliding in humid nitrogen. PhD thesis, Department of Chemical Engineering, The University of Wisconsin.

Seinfeld, J. H. 1986 *Atmospheric Chemistry and Physics of Air Pollution*. John Wiley.

Stone, H. A., Bentley, B. J. & Leal, L. G. 1986 An experimental study of transient effects in the breakup of viscous drops. *J. Fluid Mech.* **173**, 131.

Stone, H. A. & Leal, L. G. 1989 Relaxation and breakup of an initially extended drop in an otherwise quiescent fluid. *J. Fluid Mech.* **198**, 399.

Unverdi, S. O. & Tryggvason, G. 1992 A front-tracking method for viscous incompressible, multi-fluid flows. *J. Comput. Phys.* **100**, 25.